Geotechnical Effects of the 2015 Magnitude 7.8 Gorkha, Nepal, Earthquake and Aftershocks

by Robb E. S. Moss, Eric M. Thompson, D. Scott Kieffer, Binod Tiwari, Youssef M. A. Hashash, Indra Acharya, Basanta Raj Adhikari, Domniki Asimaki, Kevin B. Clahan, Brian D. Collins, Sachindra Dahal, Randall W. Jibson, Diwakar Khadka, Amy Macdonald, Chris L. M. Madugo, H. Benjamin Mason, Menzer Pehlivan, Deepak Rayamajhi, and Sital Uprety

ABSTRACT

This article summarizes the geotechnical effects of the 25 April 2015 **M** 7.8 Gorkha, Nepal, earthquake and aftershocks, as documented by a reconnaissance team that undertook a broad engineering and scientific assessment of the damage and collected perishable data for future analysis. Brief descriptions are provided of ground shaking, surface fault rupture, landsliding, soil failure, and infrastructure performance. The goal of this reconnaissance effort, led by Geotechnical Extreme Events Reconnaissance, is to learn from earthquakes and mitigate hazards in future earthquakes.

INTRODUCTION

Geotechnical Extreme Event Reconnaissance (GEER) is an organization with the goal of documenting geotechnical effects from extreme events, including earthquakes and other natural disasters. Following the **M** 7.8 event, GEER mobilized two reconnaissance teams to collect perishable data on the geotechnical effects of the 25 April 2015 Gorkha, Nepal, earthquake. The following observations and data were collected:

- the absence or presence of surface fault ruptures,
- triggered landslides,
- liquefaction and other soil-failure mechanisms, and
- geotechnical-related damage to infrastructure.

The initial GEER team surveyed the large affected area by car due to bans on flying (following an in-country U.S. helicopter crash) and on unmanned aerial vehicles (UAVs; due to unauthorized use by others immediately following the earthquake). The initial GEER team covered a broad region ranging from Pokhara in the west to Charikot in the east and from the Tibet border in the north to the India border in the south (Fig. 1). By the time the follow-up team arrived, the flying ban had been lifted and team members were able to use helicopters and UAVs (after receiving permission) to observe regions that could not be reached by car.

This article presents a summary of the full GEER report on the 2015 Gorkha earthquake sequence that can be found at www.geerassociation.org/GEER_Post%20EQ%20Reports/Nepal_2015 (last accessed September 2015). Because in-depth seismology, tectonics, rupture mechanics, and other source details are contained in separate articles in this special issue, this summary focuses solely on the geotechnical aspects of the postearthquake investigations and includes only essential background information.

GEOLOGIC AND GEOMORPHIC SETTING

The Himalaya region consists of a 100-km-wide accretionary wedge underlain by a north-dipping plate boundary décollement that slips in major earthquakes. Three major thrust faults (from north to south: the inactive Main Central thrust [MCT] fault, the most likely inactive Main Boundary thrust [MBT] fault, and the active Main Frontal thrust [MFT] fault) converge at depth into a single major shear zone, the Main Himalayan thrust (MHT), along which the Indian crust is thrust beneath Eurasia (Bollinger *et al.*, 2006). The MCT marks the southern boundary of the High Himalaya, composed of highly metamorphosed, amphibolite-grade schist with intrusive granitic plutons attributed to an accreted terrane (Robinson *et al.*, 2001). The MBT bounds the Lesser Himalaya, which are composed primarily of folded, medium-to-low-grade metasediments (DeCelles *et al.*, 2001). The MFT marks the southern boundary of the sub-Himalaya, which is generally composed of several kilometers of Tertiary siltstones, sandstones, and conglomerates that have been scraped off the Precambrian Indian basement. Great earthquakes in the Himalaya rupture to the surface along the MFT, whereas large earthquakes, such as the 2015 Gorkha earthquake, are blind ruptures limited to the MHT. The Kathmandu Valley (Fig. 1b) is unique within the Lesser Himalaya because it is a deep sedimentary basin, structurally defined by thrust faulting on the north and the south. Neogene to Quaternary sediments as thick as 500 m predominantly formed in lacustrine and fluvial depositional environments within the basin. The stratigraphy consists mainly of interbedded clays and silts with some sands and gravels (Piya, 2004).

 doi: 10.1785/0220150158

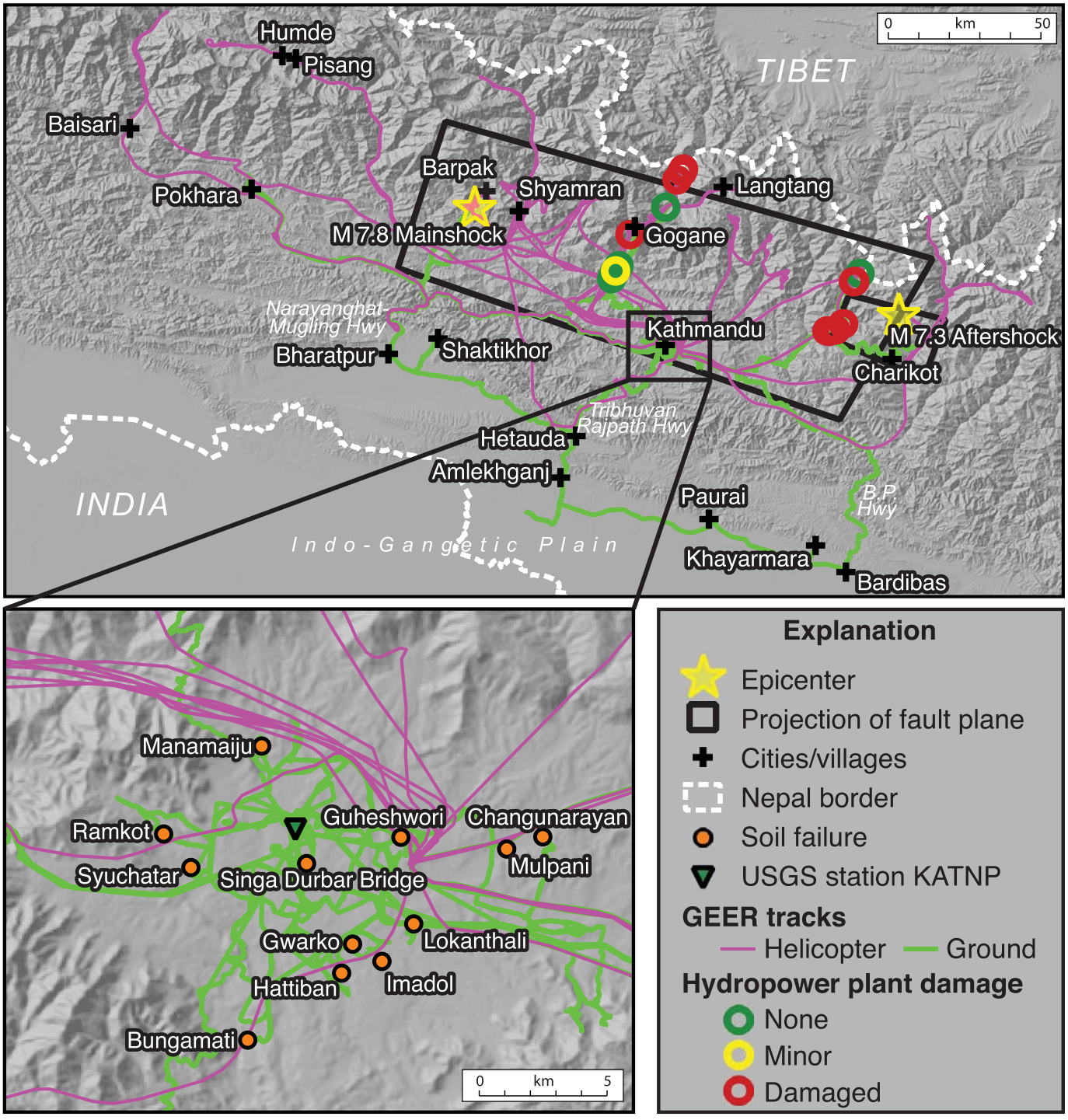

▲ **Figure 1.** (a) The epicenters and extent of the surface projection of the fault planes for the **M** 7.8 mainshock and **M** 7.3 aftershock, selected cities and villages referenced in this article, the Global Positioning System (GPS) tracks of the Geotechnical Extreme Event Reconnaissance (GEER) teams, and a simplified representation of the observed damage to hydropower projects. There are more hydropower symbols than there are hydropower projects visited by GEER, because we visited multiple sites (e.g., headworks, penstocks, dams, and powerhouses) associated with each hydropower project. (b) Enlarged view of the Kathmandu Valley shows the locations of soil failure investigated by GEER and the location of U.S. Geological Survey (USGS) station KATNP in Kathmandu. The basemap relief is from Jarvis *et al.* (2008).

GROUND MOTIONS AND SITE RESPONSE

The 2015 earthquake sequence was poorly recorded; and, as of the date of this publication, only one strong-motion recording has been made available to the greater scientific community (station KATNP, administered by the U.S. Geological Survey [USGS]; location given in Fig. 1b). (Other strong-motion instruments apparently recorded the earthquakes, but an embargo of the data has precluded access). The lack of near-source instrumental records highlights the importance of macroseimicity as the only means for quantifying the shaking intensity; this is discussed in detail by Martin *et al.* (2015). Despite the large magnitude of the 25 April 2015 mainshock (**M** 7.8) and the short distance from Kathmandu to the rupture plane (~10 km), station KATNP exhibited anomalously low energy at short periods (< 1 s). This is consistent with the findings of Martin *et al.* (2015), which show that, relative to the Szeliga *et al.* (2010) empirical equations, the shaking intensity was lower than expected at short distances (< 100 km) but consistent with expectations at larger distances (> 100 km). Figure 2 shows the rotation-independent response spectral acceleration RotD50 (Boore, 2010) against the Boore *et al.* (2014) ground-motion prediction equations (GMPEs) for both the **M** 7.8 mainshock and **M** 7.3 aftershock. Although the Boore *et al.* (2014) equations were developed primarily with ground motions from the western United States (WUS), they provide an approximate analog to Nepal because both are active crustal regions. Similarly, the GMPE selection scheme employed by ShakeMap (Garcia *et al.*, 2012) uses a WUS GMPE for this region. The Boore *et al.* (2014) equations predict a peak ground acceleration (PGA) of 0.49*g* for the **M** 7.8 earthquake, which is much higher than the recorded PGA of 0.16*g*. Because of the data paucity, however, the factors that shaped the amplitude and frequency content of the mainshock are still poorly understood.

The low amplitude of short-period shaking in the mainshock is a peculiar characteristic of this event. The observation that the short-period energy of the **M** 7.3 aftershock is well modeled by Boore *et al.* (2014) is evidence that the lack of short-period energy is related to the specific source process of the **M** 7.8 mainshock rather than the properties of the crust or basin. Although the response spectrum of the mainshock appears to be rich in energy at long periods, the comparison to Boore *et al.* (2014) shows that it is not especially large for an earthquake of this size recorded at a soft soil site. For the comparisons in Figure 2, we assume the time-averaged shear-wave velocity in the upper 30 m (V_{S30}) is 200 m/s, based on horizontal-to-vertical ratios at station KATNP by Paudyal *et al.* (2012).

FAULT RUPTURE

Extensive ground-based field investigations of the MFT and MBT were conducted by members of the GEER team, as well as by other researchers (Angster *et al.*, 2015). The ground tracks in Figure 1 indicate where we looked for surface rupture during our investigation. The MBT was observed along the Narayanghat–Mugling Highway north of Bharatpur and near the village of Shaktikhor, along the Tribhuvan Rajpath Highway north of the town of Hetauda, and along the B.P. Highway north of Bardibas (Fig. 1). No evidence of surface rupture or associated ground deformation, such as ground warping or tilting, was identified by the GEER team or reported by residents. Other effects of the earthquake, such as elevated groundwater levels and substantially increased spring and streamflow volumes, were reported in the watersheds all along the MBT for more than several weeks following the 25 April 2015 Gorkha earthquake.

The MFT is well expressed south of the MBT along the east–west-trending Siwalik Hills of the sub-Himalaya. The Tertiary sedimentary material is easily erodible but forms steep relief, demonstrating the active deformation associated with the MFT. Field reconnaissance along the MFT from Chitwan National Park (west of Hetauda) to Bardibas (Fig. 1) did not reveal any evidence for surface-fault rupture or associated ground deformation. Several large drainages exposing the MFT scarp were explored, including drainages near the towns of Amlekhganj, Paurai, and Khayarmara. Thrust faulting within the Tertiary materials was observed in many of these exposures, but no surface deformation related to the Gorkha earthquake was distinguished.

Paleoseismic data suggest that earthquakes in 1255 and 1934 ruptured to the surface along the MFT, south of Kathmandu (Bollinger *et al.*, 2014). Field observations after the 2015 rupture, which nucleated on MHT (Avouac *et al.*, 2015), suggest the rupture only extended to the base of the MFT. These findings are consistent with the magnitude dependence of surface rupture for events in this region, where surface rupture has resulted from the **M** > 8 events (e.g., 1255 and 1934) but not the **M** < 8 events (e.g., 1803, 1833, 1905, and 2015).

LANDSLIDES

Landslides triggered by strong shaking were the dominant geotechnical effect of the recent earthquakes in Nepal. Steep slopes produced by rapid tectonic uplift create high landslide hazard in Nepal even in the absence of ground shaking. Landslides triggered during the mainshock and aftershocks blocked roads, dammed rivers, and damaged villages, causing hundreds of fatalities. In some cases, rivers with landslide dams pose an ongoing hazard for downstream villages.

GEER team members investigated most major drainages in the broad epicentral region of the Gorkha earthquake sequence (specific tracks are given in Fig. 1). We observed thousands of landslides and estimate that the total number of landslides triggered is in the few tens of thousands, which includes landslides in China that were not directly investigated in the field (Collins and Jibson, 2015). This estimate is consistent with previously developed relationships between earthquake magnitude and number of landslides: the Malamud *et al.* (2004) relationship predicts about 25,000 landslides, and the Keefer (2002) relationship predicts about 60,000 landslides for an **M** 7.8 earthquake.

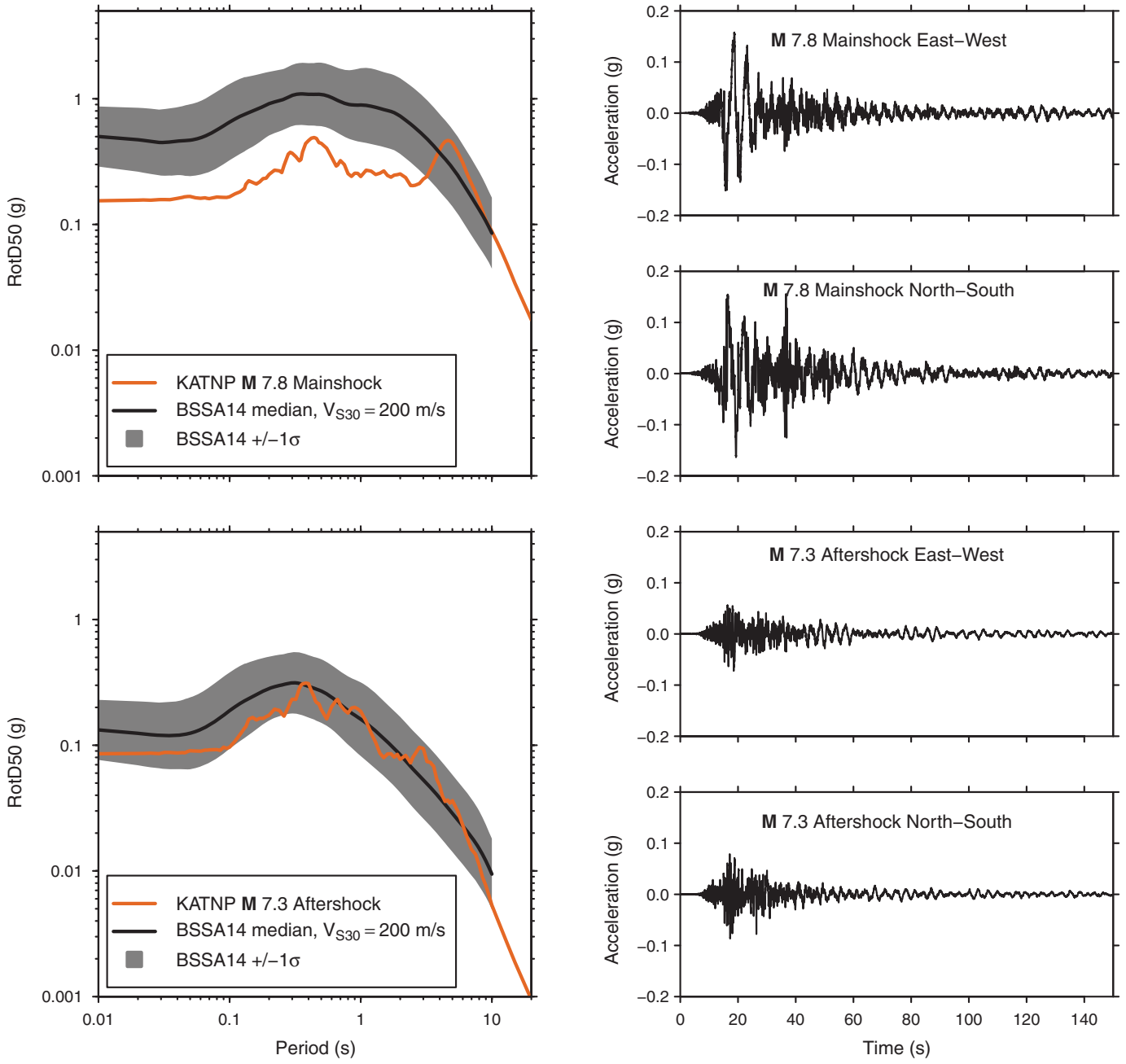

▲ **Figure 2.** Ground shaking from the (top row) **M** 7.8 Gorkha earthquake and the (bottom row) **M** 7.3 aftershock recorded at station KATNP. (Left) Orientation-independent response spectral acceleration (RodD50) compared with the Boore *et al.* (2014, labeled BSSA14) ground-motion prediction equation (GMPE). (Right) Horizontal-component time histories. V_{S30} is the time-averaged shear-wave velocity to 30 m depth.

Our estimate of the number of landslides is near the lower boundary of what would be expected from these relationships; given the steep terrain of Nepal, many more landslides may have been expected. Virtually all of the landslides were falls and slides of rock and soil, which is consistent with observations from other worldwide earthquakes (Keefer, 1984, 2002). Although a few large debris avalanches occurred, the predominant mode of landsliding was by shallow, translational failure (Collins and Jibson, 2015).

The largest and most destructive landslide resulting from the earthquakes was the Langtang debris avalanche (see map in Fig. 1; photo in Fig. 3), which began as a snow and ice avalanche and entrained debris before becoming airborne off a 500-m-tall cliff. Estimates of the velocity of the airborne landslide debris approach 100 m/s (Collins and Jibson, 2015). A few outlying structures on the east end of the village were not buried but were flattened by an accompanying air blast generated by the speed and volume of the debris avalanche. In

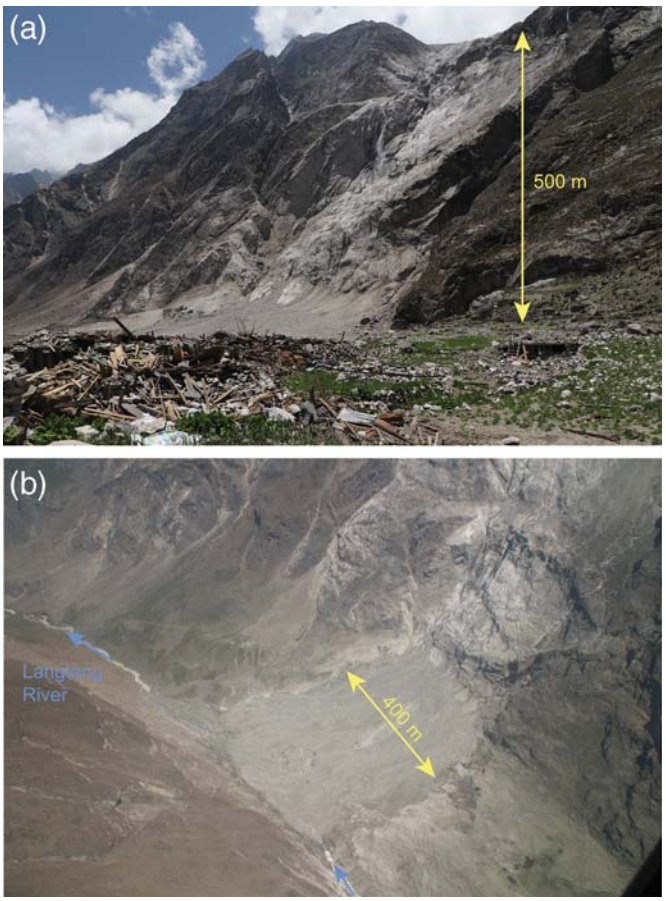

▲ **Figure 3.** The Langtang debris avalanche (28.2121° N, 85.4991° E), which destroyed the entire village of Langtang either through direct impact or by consequent air blast. An estimated 200 people were killed in this single event. (a) Oblique northwest view of deposit with cliff from which the debris became airborne. Buildings in foreground were pushed over by the ensuing airblast. (b) Aerial view of deposit showing location of the Langtang River tunnel through ice and debris (blue arrows). Reproduced from Collins and Jibson (2015).

addition to destroying many structures, the air blast completely flattened the forest for about 1 km in each direction up and down the valley, as well as all the way up to the tree line on the south (opposing) valley slope. Trees were stripped of branches and bark and were laid down in a radial pattern outward from the deposit. The estimated volume of the Langtang landslide is 2, 000, 000 m^3, and the estimated number of fatalities is approximately 200 (Collins and Jibson, 2015).

Several important valley-blocking landslides also occurred, the most notable of which buried the village of Baisari on the Kali Gandaki River (Fig. 4; 28.4026° N, 83.6017° E) several weeks after the mainshock. The rockslide at Baisari, with an estimated volume of 300, 000 m^3, failed progressively. According to interviews with members of the Nepal Army, cracks were observed in the cliff following the April 2015 **M** 7.8 earthquake, and these cracks widened during the **M** 7.3 earthquake on 12 May 2015. Ten days later, rocks began falling from the cliff, prompting evacuation of Baisari. Two days after that, at about 1:00 a.m. local time on 24 May, the slope above the river failed; the resulting landslide dammed the river and buried the entire village, including 27 homes, under about 30 m of landslide debris. The lake overtopped the dam 16 hours later. Authorities were able to evacuate the downstream villages just prior to its failure.

In most cases, valley-blocking landslides that impounded lakes breached without incident. For example, the Gogane landslide (28.0857° N, 85.2274° E) with an estimated volume of 150, 000 m^3, partially breached but impounds a small lake; landslide dams that temporarily blocked the flow of the Marsyangdi River between the villages of Pisang and Humde breached naturally and did not impound lakes as of a few weeks after the earthquake. In some cases, valley-blocking landslides consisted primarily of coarse rock fragments and were permeable enough that little or no water was impounded; an example is the Shyamran rock slide (28.1387° N, 84.8507° E), with an estimated volume of 30, 000 m^3. As of the beginning of the 2015 monsoon season, some valley-blocking landslides were still in place and posed ongoing hazard during the approaching periods of high river flow. Further details are available in the full GEER report and in Collins and Jibson (2015).

SOIL FAILURE

Seismic soil-failure modes, such as liquefaction and cyclic failure, require strong shaking of weak soils. Because of the mountainous and steep terrain throughout most of Nepal, weak soils are located primarily in sedimentary basins (e.g., Kathmandu and Pokhara) and the Indo-Gangetic plain.

The GEER team observed soil failure around the Kathmandu Valley in many locations (Fig. 1b). Most of the soil failures are classified as "incipient," indicating evidence of soil failure that did not result in appreciable deformations. For example, sand boils, ground cracks, and minor building tilt ($<2°$) were observed in Manamaiju, but the buildings were not seriously damaged. Forecasts (e.g., Piya, 2004) of the amount and scale of liquefaction in the Kathmandu Valley were not realized for many possible reasons:

- the aforementioned low amplitude of high-frequency shaking from the mainshock;
- the water table potentially being deeper (due to groundwater withdrawal) than at the time of prior earthquakes and liquefaction;
- seasonal variations in the water table (the earthquake occurred near the end of the dry season when water levels were likely at their lowest levels); and
- the lacustrine sediment being insusceptible to liquefaction because of the fine grain-size distribution.

Typical soil-failure observations included sand boils, ground fissures, tilted buildings, and, in one case, root vegetables ejected out of the ground. Soil types ranged from fine sand and silty sand to low-plasticity silty clay that is locally termed "black cotton."

The depth of the water table in the Kathmandu Valley typically ranges between 1 and 9 m. The lacustrine environment of

▲ **Figure 4.** Rock slide (28.4026° N, 83.6017° E) along the Kali Gandaki River on 24 May 2015 that buried the village of Baisari and blocked the flow of the river for 16 hours nearly one month following the main earthquake shock (a,b). Progressive failure of the nearly 350-m-tall rock mass through the weathered bedrock profile is thought to have led to its eventual collapse. Reproduced from Collins and Jibson (2015).

▲ **Figure 5.** Measurement of one of the locations having the largest offsets that was observed in the Lokanthali area along the Arniko Highway (27.67439° N and 85.36267° E).

the Kathmandu Valley transitioned to a fluvial environment around the end of the last ice age (~11 ky). Surficial deposits are primarily soft, interbedded lacustrine and fluvial sediments (Piya, 2004).

Many of the soil-failure sites liquefied, as indicated by the presence of sand boils (e.g., Manamaiju, Bungamati, Changunarayan, and Mulpani). However, an interesting ground failure occurred along the Arniko Highway in Lokanthali (27.67439° N, 85.36267° E), where lateral cracks having 2-m-deep fissures and as much as 1.5 m of nearly vertical offset occurred over a large area on or near ground sloping toward a river channel (see the photo in Fig. 5 and a map of the fissures in Fig. 6). The lack of evidence for liquefaction, reports that the failure progressed slowly, and the observation that the slip surface extended into the weak black cotton clay led to an initial assessment that these failures resulted from cyclic failure (i.e., structural breakdown of clay particles) in the black cotton clay, for which lab tests indicated moderate sensitivity and a liquidity index greater than one. Subsequent trenching and hand-

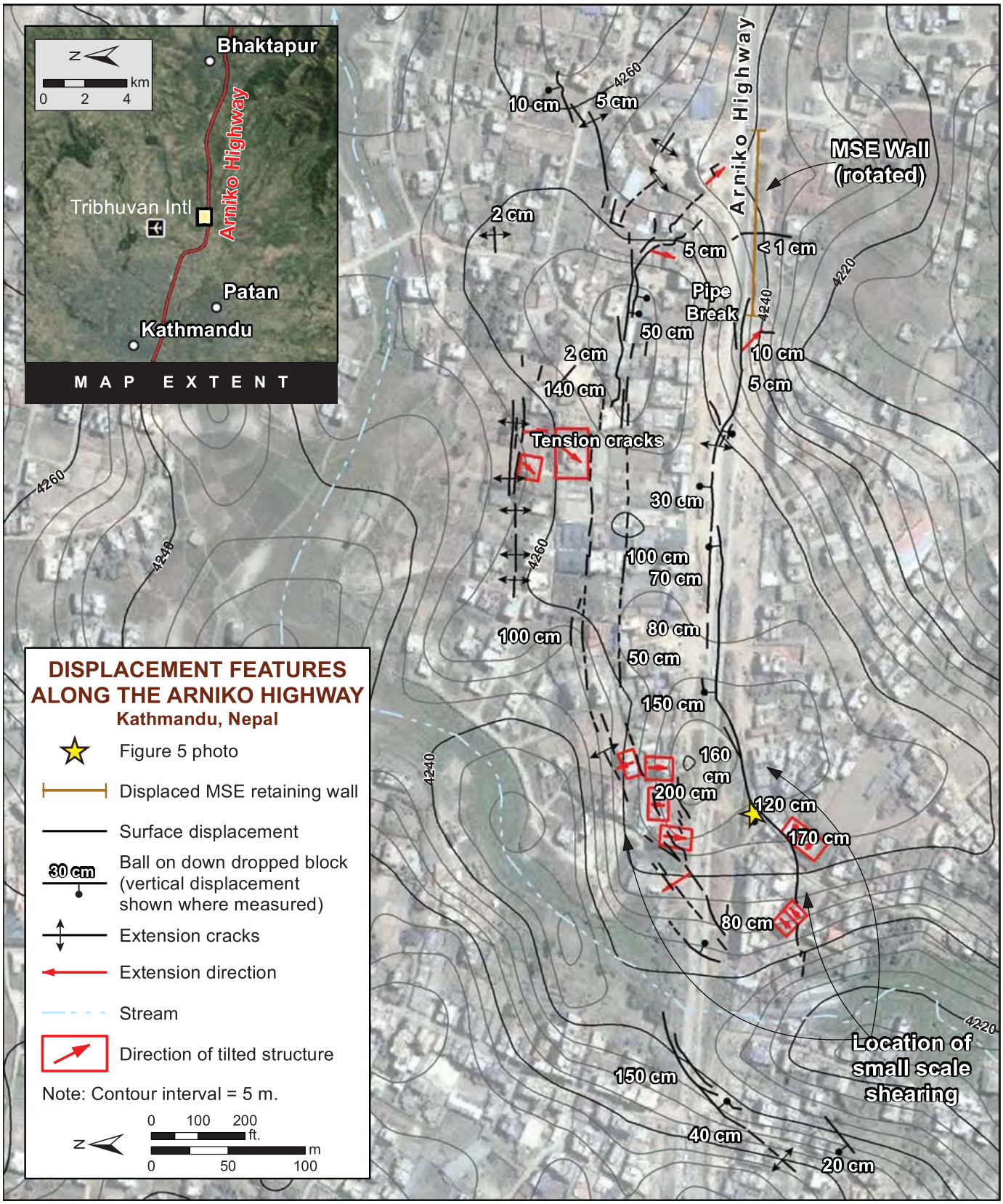

▲ **Figure 6.** Mapped ground cracks or fissures in the Lokanthali area along the Arniko Highway. Extensive cracking had lateral deformations as great as 2 m and vertical deformations as great as 1.5 m.

augering revealed more complex failure planes that were not evident on the surface. A 2.5-m-deep trench revealed buried liquefaction escape structures capped by fine-grained fluvial overbank deposits and fill layers. The 2015 slip surface appears to have offset a sand layer that had been injected from a previous event and extended down into a massive sand layer >1 m thick, suggesting that these failures are lateral spreads. It is also possible that both cyclic failure and liquefaction contributed to the soil failure in and around Lokanthali. We saw similar ground fissures in Syuchatar (27.69723° N, 85.27408° E); however, that site did not experience the large displacements observed in Lokanthali.

PERFORMANCE OF INFRASTRUCTURE

Damage to infrastructure (e.g., roads, bridges, pipelines, and dams) after earthquakes can hinder rescue, recovery, and rebuilding. Nepal's civil infrastructure is mainly composed of roads throughout the mountainous terrain, bridges crossing the numerous rivers, and hydropower facilities. In general, the infrastructure performed well in the earthquakes with some exceptions.

Few bridges were damaged. One is the Singa Durbar Bridge in downtown Kathmandu (location given in Fig. 1). It was undamaged after the mainshock, but the **M** 7.3 aftershock caused a soft-soil failure, resulting in cracks perpendicular to the right of way and parallel to the creek under the bridge. Lateral cracks in the raised concrete sidewalk sections extend on both sides of the bridge parallel to the creek and are separated by roughly 100 m along the length of the bridge.

Twenty major hydropower plants and a number of micro hydropower plants were generating 800 MW of hydropower for Nepal before the April 2015 earthquake and its aftershocks. The earthquakes damaged 16 projects totaling ~270 MW of generating capacity. The GEER team visited seven hydropower projects (Fig. 1). In the steep, narrow, upper reaches of the drainages, projects were impacted primarily by rock falls. Roads, penstocks, and secondary structures received the brunt of damage from these slope failures. In the lower reaches of the drainages, where river valleys open up and water is typically transmitted via open canals, shaking-related impacts such as settlement and structural damage was more common. The significant amount of rock-fall debris still mantling the steep upper reaches of the rivers near the epicentral areas poses a continued rock-fall hazard that will impact roads and hydropower infrastructure far into the future.

The loss of life from these earthquakes was mainly due to poor construction, generally consisting of unreinforced or poorly reinforced homes constructed of rock, brick, or concrete (BuildChange, 2015). The building codes in Nepal adequately detail how shear resistance should be incorporated into a structural design and how to avoid weak foundation soils, but enforcement of codes is poor (http://www.usaid.gov/nepal/fact-sheets/building-code-implementation-program-municipalities-nepal, last accessed September 2015). Therefore, more strictly enforced building codes could reduce loss of life in future earthquakes.

SUMMARY AND CONCLUSIONS

The **M** 7.8 Gorkha Nepal earthquake and subsequent aftershocks (including an **M** 7.3) resulted in widespread geotechnical effects due to ground shaking and subsequent soil response/failure. A summary of the reconnaissance observations made by a team sent by the GEER organization is documented here. The ground shaking in general was substantially lower in the short-period range than would be expected for an earthquake of this magnitude. The most pervasive damage was from landsliding, which buried or impacted towns, blocked rivers and streams, and closed roads and trails. Soft-soil failure was observed in and around Kathmandu in the form of liquefaction of sandy soils and cyclic failure of clayey soils. Because much of the liquefaction was marginal, this could be a very useful event to constrain liquefaction models if more of the existing ground-motion records are made available. There was no surface-fault rupture from the main event or aftershocks. Civil infrastructure withstood the earthquake shaking well, but many roads and hydropower facilities were damaged by triggered landslides.

ACKNOWLEDGMENTS

The following people and organizations contributed to this reconnaissance effort: National Science Foundation (NSF); U.S. Geological Survey (USGS); United States Agency for International Development; National Society for Earthquake Technology-Nepal; Kadoorie Agriculture Aid Association; University of Illinois at Urbana-Champaign CEE Rapid Response Grant; Mueser Rutledge Consulting Engineers; Lettis Consultants International, Inc.; Pacific Gas and Electric Company; Oregon State University; California State University (Fullerton and California Polytechnic at San Louis Obispo), Tribhuvan University (Institute of Engineering); Nepal Geotechnical Engineering Society; Kathmandu University; Department of Electricity Development, Nepal; Department of Roads, Nepal; Ministry of Physical Infrastructure and Roads; Nepal Electricity Authority; Jon Bray; Maja Bitenc; Mirjam Ziselsberger; Sanjib Basnet; Surendra Awasthi; Vijay Mahato; and Monica Maharjan. Jiaxin Xu collated the data on damage to structures in the Kathmandu Valley. Alexander Remar helped prepare Figure 6. Reviews by Robert Kayen, Kate Allstadt, Susan Hough, and an anonymous reviewer have substantially improved this article.

REFERENCES

Angster, S., E. Fielding, S. Wesnousky, I. Pierce, D. Chamlagain, D. Gautam, B. N. Upreti, Y. Kumahara, and T. Nakata (2015). Field Reconnaissance after the 25 April 2015 **M** 7.8 Gorkha earthquake, *Seismol. Res. Lett.* **86,** no. 6, doi: 10.1785/0220150135.

Avouac, J. P., L. Meng, S. Wei, T. Wang, and J. P. Ampuero (2015). Lower edge of locked Main Himalayan thrust unzipped by the 2015 Gorkha earthquake, *Nat. Geosci.*, doi: 10.1038/ngeo2518.

Bollinger, L., P. Henry, and J. P. Avouac (2006). Mountain building in the Nepal Himalaya: Thermal and kinematic model, *Earth Planet. Sci. Lett.* **244,** 58–71.

Bollinger, L., S. N. Sapkota, P. Tapponnier, Y. Klinger, M. Rizza, J. Van der Woerd, J. R. Tiwari, R. Pandey, A. Bitri, and S. Bes de Berc (2014). Estimating the return times of great Himalayan earthquakes in eastern Nepal: Evidence from the Patu and Bardibas strands of the Main Frontal thrust, *J. Geophys. Res.* **119,** 7123–7163, doi: 10.1002/2014JB010970.

Boore, D. M. (2010). Orientation-independent, nongeometric-mean measures of seismic intensity from two horizontal components of motion, *Bull. Seismol. Soc. Am.* **100,** 1830–1835.

Boore, D. M., J. P. Stewart, E. Seyhan, and G. M. Atkinson (2014). NGA-West 2 equations for predicting PGA, PGV, and 5%-damped PSA for shallow crustal earthquakes, *Earthq. Spectra* **30,** 1057–1085.

BuildChange (2015). *Post Disaster Report—Nepal*, http://www.buildchange.org/wp-content/uploads/2015/06/2015-Nepal-EQ-Reconnaissance-Report_Build-Change.pdf (last accessed September 2015).

Collins, B. D., and R. W. Jibson (2015). Assessment of existing and potential landslide hazards resulting from the April 25, 2015 Gorkha, Nepal earthquake sequence, *U.S. Geol. Surv. Open-File Rept. 2015–1142*, 50 pp., doi: 10.3133/ofr20151142.

DeCelles, P. G., D. M. Robinson, J. Quade, T. P. Ojha, C. N. Garzione, P. Copeland, and B. N. Upreti (2001). Stratigraphy, structure, and tectonic evolution of the Himalayan fold-thrust belt in western Nepal, *Tectonics* **20,** 487–509.

Garcia, D., D. J. Wald, and M. G. Hearne (2012). A global earthquake discrimination scheme to optimize ground motion prediction equation selection, *Bull. Seismol. Soc. Am.* **102,** 185–203.

Jarvis, A., H. I. Reuter, A. Nelson, and E. Guevara (2008). *Hole-filled SRTM for the Globe Version 4*, available from the CGIAR-CSI SRTM 90m Database, http://srtm.csi.cgiar.org (last accessed September 2015).

Keefer, D. K. (1984). Landslides caused by earthquakes, *Geol. Soc. Am. Bull.* **95,** 406–421.

Keefer, D. K. (2002). Investigating landslides caused by earthquakes—A historical review, *Surv. Geophys.* **23,** 473–510.

Malamud, B. D., D. L. Turcotte, F. Guzzetti, and P. Reichenbach (2004). Landslide inventories and their statistical properties, *Earth Surf. Process. Landf.* **29,** 687–711.

Martin, S. S., S. E. Hough, and C. Hung (2015). Ground motions from the 2015 **M** 7.8 Gorkha, Nepal, earthquake constrained by a detailed assessment of macroseismic data, *Seismol. Res. Lett.* **86,** no. 6, doi: 10.1785/0220150138.

Paudyal, Y. R., R. Yatabe, N. P. Bhandary, and R. K. Dahal (2012). A study of local amplification effect of soil layers on ground motion in the Kathmandu Valley using microtremor analysis, *Earthq. Eng. Eng. Vib.* **11,** 257–268.

Piya, B. K. (2004). Generation of a geological database for the liquefaction hazard assessment in Kathmandu valley, *Thesis in partial fulfillment of MS*, International Institute for Geo-Information Science and Earth Observation, Enschede, The Netherlands.

Robinson, D. M., P. G. DeCelles, P. J. Patchett, and C. N. Garzione (2001). The kinematic evolution of the Nepalese Himalaya interpreted from Nd isotope, *Earth Planet. Sci. Lett.* **192,** 507–521.

Szeliga, W., S. E. Hough, S. Martin, and R. Bilham (2010). Intensity, magnitude, location, and attenuation in India for felt earthquakes since 1762, *Bull. Seismol. Soc. Am.* **100,** 570–584.

Robb E. S. Moss
California Polytechnic State University
Department of Civil and Environmental Engineering 13-217
San Luis Obispo, California 93407-0353 U.S.A.

Eric M. Thompson
Randall W. Jibson
U.S. Geological Survey
1711 Illinois Street
Golden, Colorado 80401 U.S.A.
emthompson@usgs.gov

D. Scott Kieffer
Graz University of Technology
Institute of Applied Geosciences
Rechbauerstrasse 12
8010 Graz, Austria

Binod Tiwari
California State University, Fullerton
College of Engineering and Computer Science
800 N State College Boulevard, E-419
Fullerton, California 92834 U.S.A.

Youssef M. A. Hashash
University of Illinois at Urbana-Champaign
2230c Newmark Civil Engineering Laboratory
205 N. Mathews Avenue
Urbana, Illinois 61801 U.S.A.

Indra Acharya
Basanta Raj Adhikari
Tribhuvan University
Department of Civil Engineering
Institute of Engineering
Pulchowk Campus
Pulchowk, Lalitpur
P.O. Box 1175, Nepal

Domniki Asimaki
California Institute of Technology
1200 E. California Boulevard
MC 104-44
Pasadena, California 91125 U.S.A.

Kevin B. Clahan
Lettis Consultants International, Inc.
1981 N. Broadway, Suite 330
Walnut Creek, California 94596 U.S.A.

Brian D. Collins
U.S. Geological Survey
345 Middlefield Road, MS973
Menlo Park, California 94025 U.S.A.

Sachindra Dahal
University of Illinois at Urbana-Champaign
B235 Newmark Civil Engineering Laboratory
Urbana, Illinois 61801 U.S.A.

Diwakar Khadka
Material Test Pvt. Ltd.
Mid-Baneshwor
G.P.O. Box 1274
Kathmandu, Nepal

Amy Macdonald
Thornton Tomasetti
51 Madison Avenue
New York, New York 10010 U.S.A.

Chris L. M. Madugo
Pacific Gas and Electric Company
Mail Code N4C, Room 422A
P.O. Box 770000
San Francisco, California 94177 U.S.A.

H. Benjamin Mason
Deepak Rayamajhi
Oregon State University
School of Civil and Construction Engineering
1491 SW Campus Way
Corvallis, Oregon 97331 U.S.A.

Menzer Pehlivan
Mueser Rutledge Consulting Engineers
225 West 34th Street
New York, New York 10122 U.S.A.

Sital Uprety
University of Illinois at Urbana-Champaign
205 N. Mathews Avenue
4158 Newmark Lab, MC 250
Urbana, Illinois 61801 U.S.A.